

Supporting Information

Cavity Catalysis: Modifying Linear Free-energy Relationship under Cooperative Vibrational Strong Coupling

Jyoti Lather,[†] Thabassum Ahammad N. K.,[†] Jaibir Singh, and Jino George*

Indian Institute of Science Education and Research (IISER) Mohali
Punjab-140306, India.

*E-mail: jgeorge@iisermohali.ac.in

[†]These authors contributed equally.

CONTENTS

SL. No.	Name of the Section	Page No.
1	Experimental methods	S2
2	Synthesis of ester derivatives	S2
3	Characterisation of ester derivatives	S3
4	Kinetic analysis	S4
5	Thermodynamic analysis	S6
6	Solvent and coupling strength effect on cooperative VSC	S11

1. Experimental methods:

The experimental setup we used to study vibrational strong coupling is a Fabry-Perot (FP) cavity illustrated in figure 2. The mirrors incorporated in the cavity are usually made by substrates like BaF₂, CaF₂, ZnSe, Glass, Quartz, etc. These substrates need to be transparent enough to facilitate our probing method. In the current study, we used BaF₂ windows, as it is evident both in IR and UV-VIS regions (200 to 10000 nm). Each BaF₂ substrate was coated with Au mirrors (10 nm) to create the FP cavity. These mirrors were placed in a demountable flow cell holder with a mylar spacer of 12 μm. After assembling the mirrors in the demountable holder, the path length can be controlled by the screws. The naked eye can see a homogeneous area between the mirrors forming the so-called Newton ring and the same has been analysed in the transmission mode using a FTIR spectrometer. UV-Visible spectrophotometer used to probe the tiny homogeneous area of the cavity using an appropriate cache. The cavity mode position can be tuned by evenly moving the screws on the sample holder. The transmission spectrum of Au mirror reflection in the far IR region is used to calculate the cavity's Q-factor, which is ~60 for the 7th mode of the cavity. Full-width half maxima (FWHM) is 30 for this cavity mode, which matches to the C=O_{str} vibrational band.

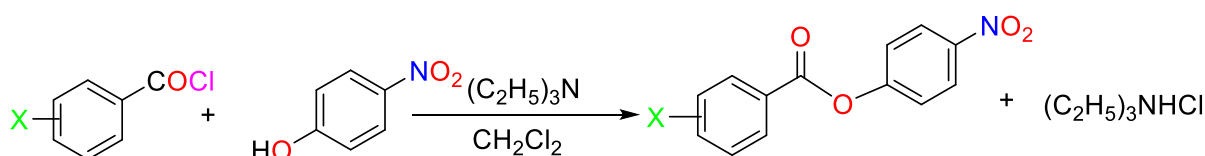
An empty cavity is referred to as air filled system, where the refractive index ($n=1$), pathlength ($L = 12\mu\text{m}$) and calculated the free spectral range (FSR). The distance between the mirrors is adjustable by choosing a suitable mylar spacer. Frequency difference or free spectral range (k) between two successive cavity modes can be obtained from the following equation

$$k = \frac{1}{2nL}$$

2. Synthesis of ester derivatives:

All benzoate ester derivatives were prepared in-situ according to a reported synthetic route. 0.07 g of p-nitrophenol (5 mmol) and .57 g triethylamine (5 mmol) were taken in an Erlenmeyer flask, and 30 mL of dichloromethane (DCM) was added into the solution. After gently dissolving the compounds, the substituted benzoyl chloride of our choice, dissolved in 10 mL of DCM and slowly added. The mixture was stirred for over 30 minutes at room temperature. After this, 20 mL of water was added to the reaction mixture and transferred to a separatory funnel, and removed the aqueous phase. It was followed by washing the organic phase once with HCl (20 mL), twice with 5% NaHCO₃ (20 mL), and once with brine solution (20 mL). After this, the organic phase dried by added Na₂CO₄. The mixture is then transferred

to a round bottom flask to remove the solvent using for rotary evaporation. Used ethanol to recrystallize the product formed. ^1H NMR using to characterized the benzoate esters spectroscopy using CDCl_3 as solvent. Synthesizing all molecules are in-situ used in the study. Derivative benzoyl chloride with para-nitrophenol dissolved in dichloromethane in the presence of triethylamine for 30 minutes (Scheme S1), followed by product separation and recrystallization from ethanol. All reactions produced a good yield. Later, benzoate esters formed were characterized with ^1H NMR (CDCl_3), FT-IR, and melting point and validated with literature reports.



Six compounds with varied substituents at meta and para positions in the structure were synthesized shown in Scheme S1. The substituents are X=H, X= m-CH₃, X= p-CH₃, X= m-OCH₃, X= m-Cl, and X= p-Cl.

3. Characterisation of ester derivatives:

p-nitrophenyl benzoate: ^1H NMR (400 MHz, CDCl_3), δ 8.36 (d, J = 8.8 Hz, 2H), 8.23 (d, J = 7.92 Hz, 2H), 7.71(t, J = 7.2 Hz, 1H), 7.57(t, J = 7.6 Hz, 2H), 7.45(d, J = 8.88 Hz, 2H)

p-nitrophenyl m-toluate: ^1H NMR (400 MHz, CDCl_3), δ 8.35 (d, J = 8.84 Hz, 2H), 8.03(d, J = 8.2 Hz, 2H), 7.52-7.43(m, 4H), 2.49(s, 3H)

p-nitrophenyl p-toluate: ^1H NMR (400 MHz, CDCl_3), δ 8.34 (d, J = 8.76 Hz, 2H), 8.11 (d, J = 7.92 Hz, 2H), 7.43 (d, J = 8.8 Hz, 2H), 7.36 (d, J = 7.92 Hz, 2H), 2.49 (s, 3H)

p-nitrophenyl m-anisate: ^1H NMR (400 MHz, CDCl_3), δ 8.33 (d, J = 9.2 Hz, 2H), 7.8(dt, J = 8.7 Hz, 1H), 7.68 (dd, J = 1.6 Hz, J = 2.4 Hz), 7.46-7.4(m, 3H), 7.22 (dddd, J = 1.28 Hz, J = 3 Hz, J = 3.96 Hz, J = 8.68 Hz), 3.69 (s, 3H)

p-nitrophenyl m-chlorobenzoate: ^1H NMR (400 MHz, CDCl_3), δ 7.36(d, J = 9.16 Hz), 2 H), 8.2 (t, J = 1.72 Hz, 1H), 8.11 (dt, J = 1.16 Hz, J = 2.52 Hz, J = 7.82 Hz, 1H), 7.68 (dq, J = 1 Hz, J = 2.04 Hz, J = 3.08 Hz, J = 8.04 Hz, 1H), 7.52(t, J = 7.92 Hz, 1H), 7.44(d, J = 9.12 Hz, 2H)

p-nitrophenyl p-chlorobenzoate: ^1H NMR (400 MHz, CDCl_3), δ 8.35 (d, $J = 9.2$ Hz, 2H), 8.16 (d, $J = 8.72$ Hz, 2H), 7.54 (d, $J = 7.88$ Hz, 2H), 7.44 (d, $J = 9.2$ Hz, 2H).

All the solutes (PNPB / derivative) prepared 0.1 M in isopropyl acetate and 0.1 M TBAF prepared in methanol.

4. Kinetic analysis:

Initially, the scan rate method (collecting the whole spectrum) has been used to determine the reaction kinetics. The baseline is recorded just before starting the spectral acquisition. Here, the absorption spectra from 350 nm to 500 nm were recorded with an interval of 16 seconds between each measurement (figure S1) keeping a slit bandwidth of 5 nm. More precisely, the changes in the absorbance at 400 nm (A_t) indicating the formation of *para*-nitrophenoxide ion are monitored for 10 minutes to assess the progress of the reaction. Before injecting the reaction mixture, the FSR of the cavity was precalculated by using the refractive index of the medium. Once kinetic data has acquired, the FSR is re-examined using the FTIR spectrometer.

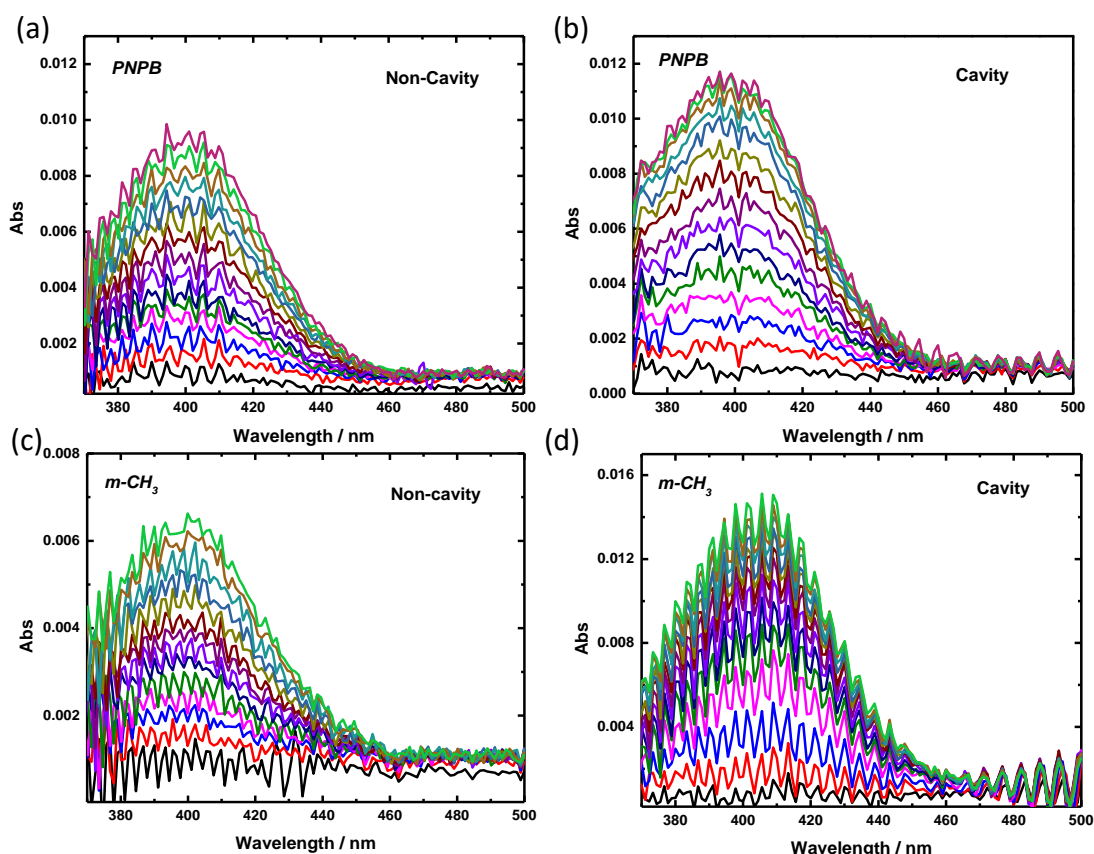


Figure S1. Scan kinetics (temporal evolution) for the formation of PNP⁻ ions from PNPB and *m*-CH₃ (a, c) non-cavity; (b, d) ON resonance cavity.

Temporal scan won't allow us to obtain the initial rate for the fast reactions (*p*-Cl, *m*-Cl). So, we collected only the wavelength trace at 400 nm with an interval of 1 second, and plotted the kinetic traces. Please note that the deadtime (the time required to start monitoring the reaction inside the cavity after mixing) of the reaction is fixed as 40 seconds for all the measurements. This longer deadtime in measurement is due to the time required for mixing and manual injection into the cavity. A first-order reaction can be represented as follows:

$$\ln\left(\frac{A_t}{A_0}\right) = -k_{app}t \quad \dots \dots (1)$$

where, A_0 and A_t are the absorbance at time zero and t , respectively. Apparent rate constant for unsubstituted molecule (PNPB):

$$k_{app} = 1.05 \times 10^{-3} \text{ sec}^{-1}$$

Consider at time t the remaining concentration of the reactant is 96%

$$A_t = 0.96A_0$$

Substitute the value of k_{app} and A_t in equation 1:

$$\ln\left(\frac{0.96A_0}{A_0}\right) = -1.05 \times 10^{-3} t$$

$$\ln(0.96) = -1.05 \times 10^{-3} t$$

$$-0.04082 = -1.05 \times 10^{-3} t$$

$$t \sim 40 \text{ sec}$$

This indicates that only 4% of the actual reaction is occurring outside the cavity. There is no deviation from the first-order rate as we are monitoring the initial rate of the reaction. A_{inf} of the reaction was obtained after 5000 seconds (roughly 10 times of half-life ($t_{1/2}$)) and found to be 0.037 OD (figure S2) for unsubstituted derivative. This A_{inf} is used for further apparent rates calculation in tuning experiments. The kinetic plot for the different derivatives is shown in figure S3.

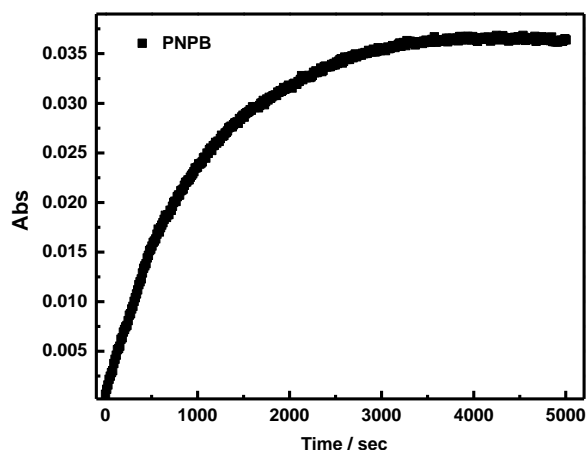


Figure S2. Formation of PNP- ions during the reaction for solvolysis PNPB (Non-cavity).

Pseudo-first-order reaction expression can be written as,

$$\ln\left(1 - \frac{A_t}{A_f}\right) = k_{app} \quad \dots \dots (2)$$

Where A_t is the absorbance at time t and A_f at infinity time, respectively. The slope of the linear regression plot of $-\ln(1 - (A_t/A_f))$ versus time gives the apparent rate, k_{app} . The reaction rate calculation has been done for initial 120 seconds. Apparent rate for the non-cavity and ON resonance cavity is given in Table 1. The light beam of the UV-Visible spectrophotometer must pass through the homogeneous area (sweet spot where the Newton ring is formed) of the cavity to obtain the kinetic traces. We recommend to use a cache to get consistency in the data acquisition. This will help a better FSR analysis and its comparison in a tuning experiment. Both scan kinetics or single point analysis was used in our experiments depending up on the speed of the reaction.

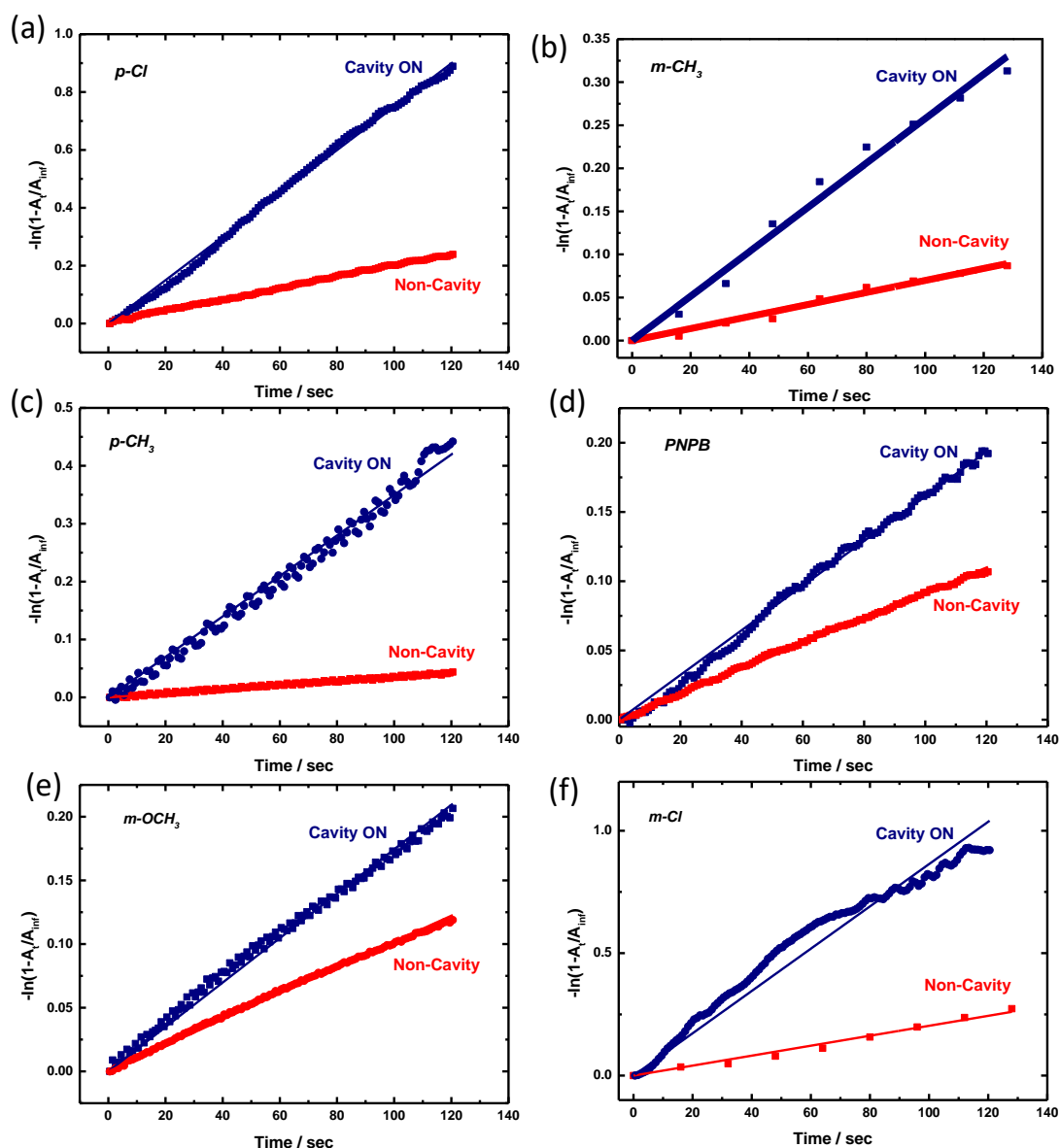


Figure S3. Reaction rate plot for non-cavity and ON- resonance cavity. (a) *p*-Cl, (b) *m*-CH₃, (c) *p*-CH₃, (d) PNPB, (e) *m*-OCH₃, (b) *m*-Cl.

5. Thermodynamic analysis:

The demountable flow cell used for the experiment is compatible with the temperature control experiments. Eyring equation is used for the calculation of activation enthalpy and entropy of the reaction for all the derivatives. Before injecting the reaction mixture, the cavity was stabilized for 30 minutes at a given temperature. All the experiments are performed in the range of 19 °C to 35 °C. Corresponding kinetic data are acquired in the same condition. For example, an interval of 1 second is used to measure the PNP- formation at 400 nm for both cavity and

non-cavity experiments. Please note that the linear plot is scattered in some cases (see figure S4a, d and h) due to instrument response while acquiring the data. Here, the relative standard deviation (RSD) is within a maximum limit of 16 %. This change is negligible compared to the actual enhancement due to vibrational strong coupling (more than 500 to 700%). Linear regression fit is done by taking the Y-intercept as zero for consistency.

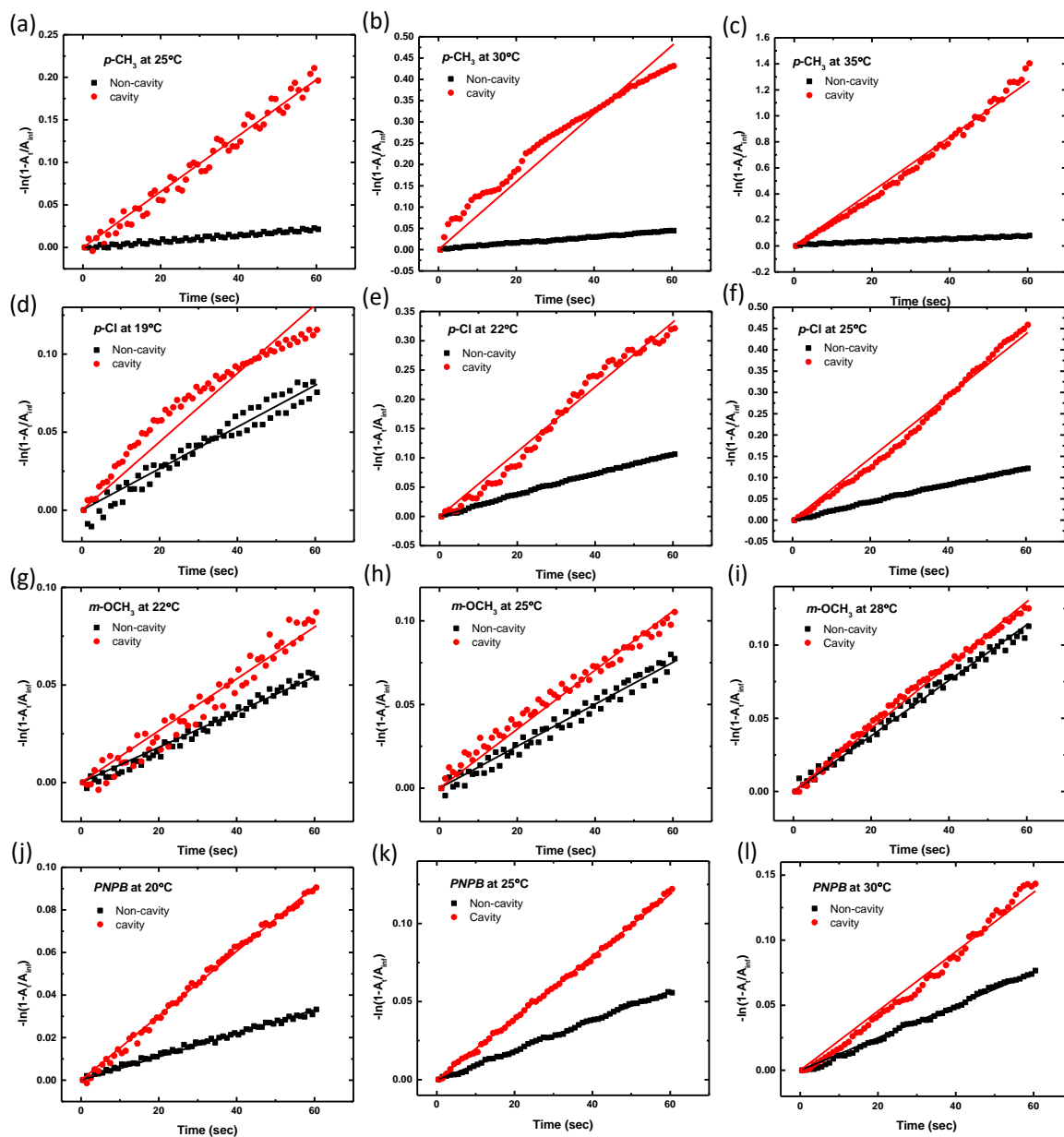


Figure S4. A comparison of kinetic plot for different temperature of non-cavity and cavity; (a,b,c) $p\text{-CH}_3$, (d,e,f) $p\text{-Cl}$, (g,h,i) $m\text{-OCH}_3$, (j,k,l) PNPB .

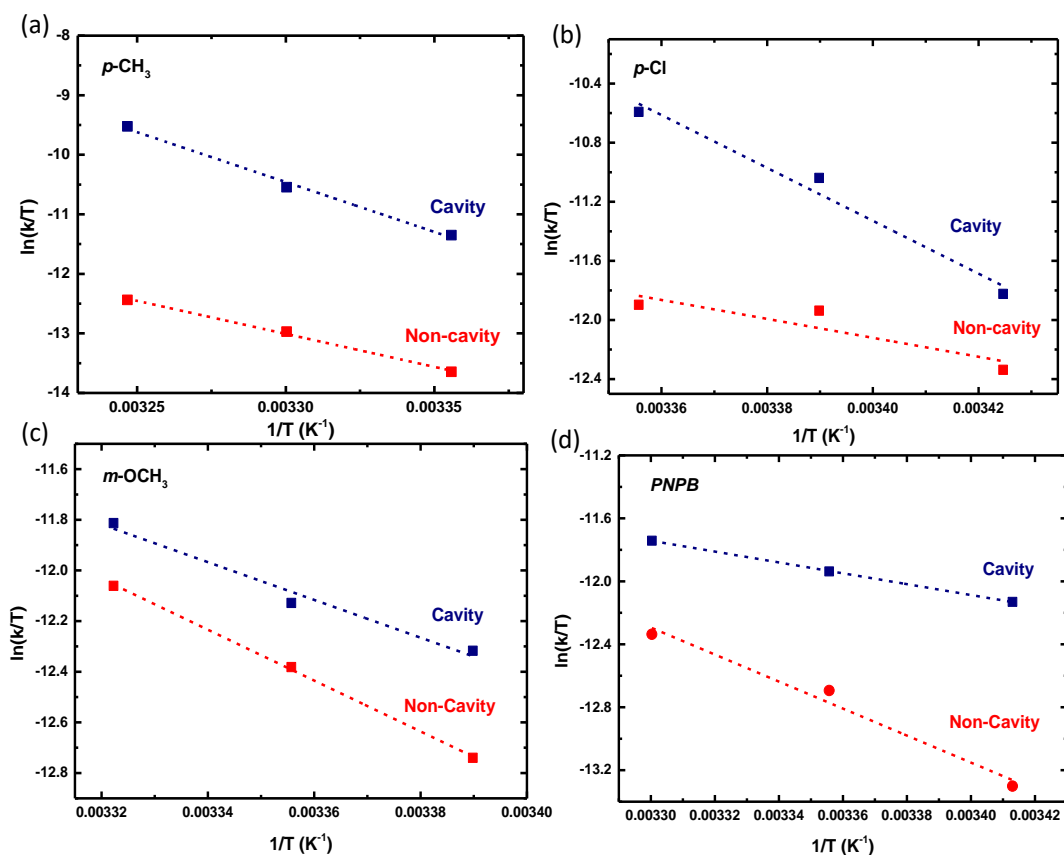


Figure S5. Temperature dependence experiment for non-cavity and cavity;(a) $p-CH_3$, (b) $p-Cl$, (c) $m-OCH_3$, (d) $PNPB$.

Calculation for enthalpy and entropy shown in figure S5:

$$k = \frac{k_B T}{h} \exp\left(\frac{-\Delta H^\ddagger}{RT} + \frac{\Delta S^\ddagger}{R}\right)$$

From figure S5:

(a) Non-cavity ($p-CH_3$)

$$\frac{-\Delta H^\ddagger}{R} = -9519.77 \text{ (slope)}$$

$$\Delta H^\ddagger = 79.15 \text{ kJmol}^{-1}$$

$$\ln\left(\frac{k_B}{h}\right) + \frac{\Delta S^\ddagger}{R} = 18.43 \text{ (intercept)}$$

$$\ln\left(\frac{k_B}{h}\right) = 23.76 \text{ (constant)}$$

$$\Delta S^\ddagger = -44.31 \text{ JK}^{-1}\text{mol}^{-1}$$

Cavity (p-CH₃)

$$\frac{-\Delta H^\ddagger}{R} = -16751.34 \text{ (slope)}$$

$$\Delta H^\ddagger = 139.27 \text{ kJmol}^{-1}$$

$$\ln\left(\frac{k_B}{h}\right) + \frac{\Delta S^\ddagger}{R} = 44.82 \text{ (intercept)}$$

$$\ln\left(\frac{k_B}{h}\right) = 23.76 \text{ (constant)}$$

$$\Delta S^\ddagger = 175.07 \text{ JK}^{-1}\text{mol}^{-1}$$

$$\Delta\Delta H^\ddagger = \Delta H^\ddagger_{\text{cavity}} - \Delta H^\ddagger_{\text{cell}} = \mathbf{60.12 \text{ kJmol}^{-1}}$$

$$\Delta\Delta S^\ddagger = \Delta S^\ddagger_{\text{cavity}} - \Delta S^\ddagger_{\text{cell}} = \mathbf{219.38 \text{ JK}^{-1}\text{mol}^{-1}}$$

(b) Non-cavity (p-Cl)

$$\frac{-\Delta H^\ddagger}{R} = -6410.77 \text{ (slope)}$$

$$\Delta H^\ddagger = 53.29 \text{ kJmol}^{-1}$$

$$\ln\left(\frac{k_B}{h}\right) + \frac{\Delta S^\ddagger}{R} = 9.67 \text{ (intercept)}$$

$$\ln\left(\frac{k_B}{h}\right) = 23.76 \text{ (constant)}$$

$$\Delta S^\ddagger = -117.12 \text{ JK}^{-1}\text{mol}^{-1}$$

Cavity (p-Cl)

$$\frac{-\Delta H^\ddagger}{R} = -17889.4 \text{ (slope)}$$

$$\Delta H^\ddagger = 148.73 \text{ kJmol}^{-1}$$

$$\ln\left(\frac{k_B}{h}\right) + \frac{\Delta S^\ddagger}{R} = 49.49 \text{ (intercept)}$$

$$\ln\left(\frac{k_B}{h}\right) = 23.76 \text{ (constant)}$$

$$\Delta S^\ddagger = 213.93 \text{ JK}^{-1}\text{mol}^{-1}$$

$$\Delta\Delta H^\ddagger = \Delta H^\ddagger_{\text{cavity}} - \Delta H^\ddagger_{\text{cell}} = \mathbf{95.44 \text{ kJmol}^{-1}}$$

$$\Delta\Delta S^\ddagger = \Delta S^\ddagger_{\text{cavity}} - \Delta S^\ddagger_{\text{cell}} = \mathbf{331.05 \text{ JK}^{-1}\text{mol}^{-1}}$$

(c) Non-cavity (m-OCH₃)

$$\frac{-\Delta H^\ddagger}{R} = -10046.83 \text{ (slope)}$$

$$\Delta H^\ddagger = 83.53 \text{ kJmol}^{-1}$$

$$\ln\left(\frac{k_B}{h}\right) + \frac{\Delta S^\ddagger}{R} = 21.32 \text{ (intercept)}$$

$$\ln\left(\frac{k_B}{h}\right) = 23.76 \text{ (constant)}$$

$$\Delta S^\ddagger = -20.29 \text{ JK}^{-1}\text{mol}^{-1}$$

Cavity (m-OCH₃)

$$\frac{-\Delta H^\ddagger}{R} = -7455.6848 \text{ (slope)}$$

$$\Delta H^\ddagger = 61.98 \text{ kJmol}^{-1}$$

$$\ln\left(\frac{k_B}{h}\right) + \frac{\Delta S^\ddagger}{R} = 12.93 \text{ (intercept)}$$

$$\ln\left(\frac{k_B}{h}\right) = 23.76 \text{ (constant)}$$

$$\Delta S^\ddagger = -90.02 \text{ JK}^{-1}\text{mol}^{-1}$$

$$\Delta\Delta H^\ddagger = \Delta H^\ddagger_{\text{cavity}} - \Delta H^\ddagger_{\text{cell}} = -21.55 \text{ kJmol}^{-1}$$

$$\Delta\Delta S^\ddagger = \Delta S^\ddagger_{\text{cavity}} - \Delta S^\ddagger_{\text{cell}} = -69.73 \text{ JK}^{-1}\text{mol}^{-1}$$

(d) Non-cavity (PNPB)

$$\frac{-\Delta H^\ddagger}{R} = -8578.51 \text{ (slope)}$$

$$\Delta H^\ddagger = 71.32 \text{ kJmol}^{-1}$$

$$\ln\left(\frac{k_B}{h}\right) + \frac{\Delta S^\ddagger}{R} = 16.02 \text{ (intercept)}$$

$$\ln\left(\frac{k_B}{h}\right) = 23.76 \text{ (constant)}$$

$$\Delta S^\ddagger = -64.42 \text{ JK}^{-1}\text{mol}^{-1}$$

Cavity (PNPB)

$$\frac{-\Delta H^\ddagger}{R} = -3449.92 \text{ (slope)}$$

$$\Delta H^\ddagger = 28.68 \text{ kJmol}^{-1}$$

$$\ln\left(\frac{k_B}{h}\right) + \frac{\Delta S^\ddagger}{R} = -0.3574 \text{ (intercept)}$$

$$\ln\left(\frac{k_B}{h}\right) = 23.76 \text{ (constant)}$$

$$\Delta S^\ddagger = -200.51 \text{ JK}^{-1}\text{mol}^{-1}$$

$$\Delta\Delta H^\ddagger = \Delta H^\ddagger_{\text{cavity}} - \Delta H^\ddagger_{\text{cell}} = -42.64 \text{ kJmol}^{-1}$$

$$\Delta\Delta S^\ddagger = \Delta S^\ddagger_{\text{cavity}} - \Delta S^\ddagger_{\text{cell}} = -136.09 \text{ JK}^{-1}\text{mol}^{-1}$$

6. Solvent and coupling strength effect on cooperative VSC:

In order to understand the effect of co-operative VSC we studied the kinetics by choosing a solvent (acetonitrile), which doesn't have a vibrational band at the C=O stretching band of the solute molecules. Acetonitrile is IR silent at 1750 cm^{-1} and reaction rate was monitored in both cavity and non-cavity conditions. Here, 0.1 M *p*-nitrophenyl *p*-toluate (*p*-CH₃) dissolved in acetonitrile and the experiment has been performed in different FSR values of the cavity (7th mode) and non-cavity after coupling the C=O_{str} band of the solute. Cavity tuning experiments suggest that the reaction rate was not affected even if the 7th mode crosses the C=O_{str} of the solute molecule. The solute is in very low concentration and hence the effective VSC is negligible. This underline effect of cooperative VSC between the solvent and the solute molecules in controlling reaction rates.

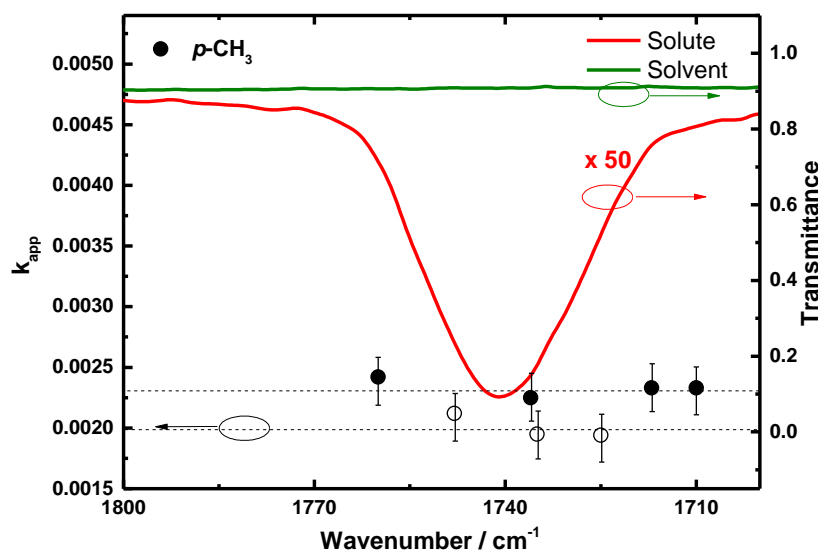


Figure S6. IR spectra of acetonitrile (green trace), solute *p*-CH₃ (red trace) and the calculated reaction rate k_{app} for detuning experiment of cavity (dark black circles) and non-cavity (empty black circles) conditions.

In a similar attempt, we looked into the effect of rate enhancement *versus* the coupling strength by varying the active solvent (IPAc) concentration. Here the initial concentration of the solute (0.1 M of p-nitrophenyl p-toluate (*p*-CH₃)) is fixed throughout the experimental condition. Different batch of solutions prepared by mixing anisole in IPAc (ranging from 33% to 100%). Changing the concentration of the C=O oscillators (IPAc) from 33% to 100% shows a non-linear behaviour in rate of the reaction, whereas, the coupling strength varies linearly with respect to square root of concentration.

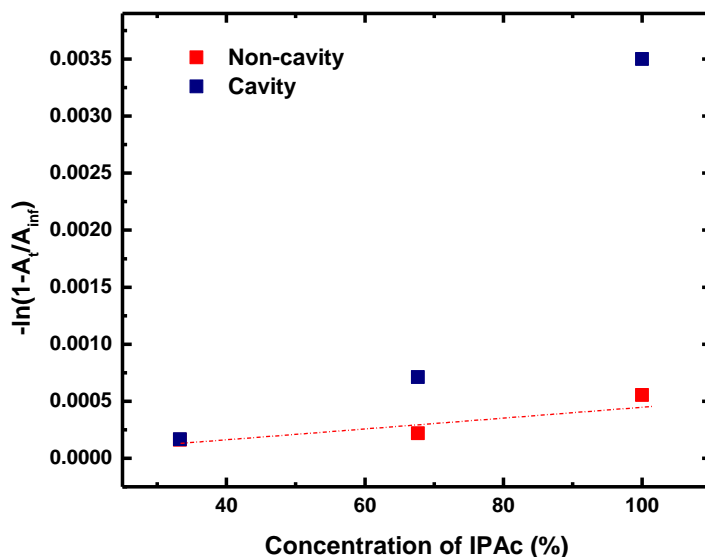


Figure S7. Concentration dependence experiment by mixing anisole and IPAc in different ratio and the corresponding reaction rate k_{app} of *p*-CH₃ for non-cavity (red squares) and ON-resonance condition (blue squares).